OPTIMIZATION OF BINARY REGRESSION TREE MODELS FOR ESTIMATING THE SPATIAL DISTRIBUTION OF SNOW WATER EQUIVALENT IN AN ALPINE BASIN

Noah P. Molotch[1], Roger C. Bales[2], Michael T. Colee[3], and Jeff Dozier[3]

ABSTRACT

Regression tree models have been shown to provide the most accurate estimates of distributed SWE when intensive field observations are available. This work presents an approach that improves regression tree model performance by optimizing the use of independent variables and by comparing different residual interpolation techniques. The analysis was performed in the 19.1 km2 Tokopah basin, located in the southern Sierra Nevada of California. Snow depth, the dependent variable of the statistical models, was derived from three snow surveys (April, May and June, 1997), with an average of 990 depth measurements per survey. Estimates of distributed SWE were derived from the product of the snow depth surfaces, the average snow density (54 measurements on average), and the fractional snow covered area (obtained from the Landsat Thematic Mapper and the Airborne Visible/Infrared Imaging Spectrometer). Inclusion of the independent variable northness improved regression tree model fit. Co-kriging with solar radiation proved to be the best method for distributing residuals for April and June, with inverse distance weighting providing the best result for May.

INTRODUCTION

It is estimated that snowmelt derived from the Sierra Nevada of California provides 75% of the state's water supply for agriculture (Rosenthal and Dozier, 1996). Currently, operational streamflow forecasts are based on empirical snowmelt runoff models that may not perform well under extreme climatic conditions. As a result, current research efforts are aimed at estimating stream discharge using physically based snowmelt runoff models. These models require distributed estimates of snow water equivalent (SWE) for model initialization. SWE estimates derived from ground observations have also been used to evaluate energy-balance snowmelt models (Cline et al., 1998) and for validating remotely sensed SWE. Binary regression trees have been used to model the spatial distribution of SWE from point observations with considerable success (Winstral et al., 2002, Balk and Elder, 2000, Elder, 1995, Elder et al., 1995). The most commonly used independent variables are net solar radiation, slope, elevation, and in some cases, vegetation type. Improvements have been obtained by the inclusion of additional independent variables representing wind redistribution of snow (Winstral et al., 2002) and a cosine transformation of aspect (Erxleben et al., 2002).

The use of geostatistical techniques to distribute regression tree model residuals has been shown to improve distributed snow depth estimates (Balk and Elder, 2000, Erxleben et al., 2002). However, poor spatial autocorrelations of residuals have been cited, which questions the appropriateness of geostatistical techniques. In the absence of spatially autocorrelated residuals the use of inverse distance weighting (IDW) becomes attractive; as variogram model fitting can be exhaustive with poor results. This research builds upon previous applications of regression tree models by identifying the best combination of independent variables and by comparing geostatistical techniques and inverse-distance weighting to distribute model residuals. Three questions are addressed. First, what combination of independent variables achieves optimal model results? Second, what is the most accurate method of distributing model residuals? Finally, what is the spatial distribution of SWE in the Tokopah basin during the 1997 field campaigns?

Paper presented Western Snow Conference 2003
[1] Department of Hydrology and Water Resources, University of Arizona, Tucson, 85721-0011
[2] Division of Engineering, University of California, Merced, 95344
[2] Donald Bren School of Environmental Science and Management, University of California, Santa Barbara, 93106

STUDY AREA

This research was conducted in the 19.1 km^2 Tokopah Basin of the Sierra Nevada, Ca. located in the alpine region of Sequoia National Park (36°36'N, 118°40W) (Figure 1). The elevation of this gauged basin ranges from 2622 to 3487 m, with granite bedrock dominant and forest cover restricted to small areas of the valley floor. Tonnessen (1991) provides a detailed description of the Emerald Lake sub-basin. Nearly all of the precipitation inputs fall as snow derived from frontal storms originating over the Pacific Ocean. The small amount of summer precipitation occurs as rainfall predominantly from convective storms.

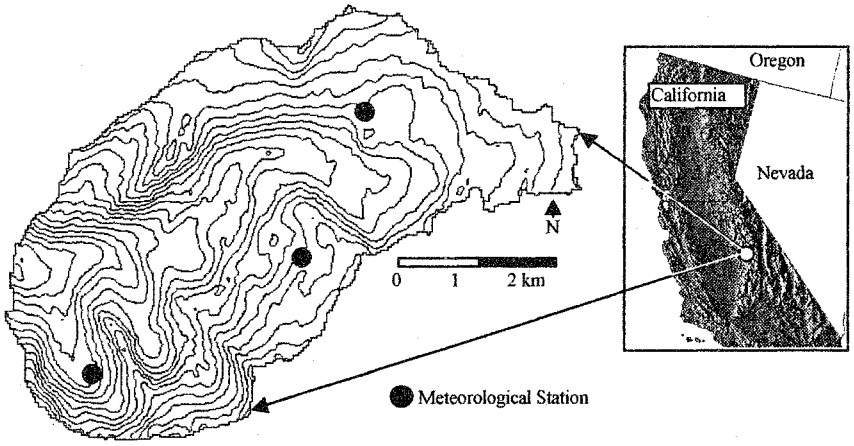

Figure 1. The Tokopah basin with 40 m contours and location of meteorological stations.

FIELD METHODS

Ground observations of snow depth and density were collected during three campaigns (April 6th – 12th, May 8th – 15th, and June 16th – 18th, 1997) (Figure 2). Depth measurements were made on a relatively evenly spaced grid pattern across the Tokopah basin, with measurement locations separated by approximately 240 m. The April, May and June snow surveys consisted of 397, 303, and 258, snow depth locations respectively. At each sampling location 3 depth measurements were collected 5 m apart along transects oriented in the direction of travel with the center measurement recorded using global positioning systems. The April, May and June surveys consisted of 19, 76 and 66 snow density measurements respectively. April snow density measurements were derived from snow pits in which samples were taken at 10 cm vertical intervals using a 1000 cc stainless steel cutter. May and June snow density measurements were made using a Federal Sampler.

MODELING METHODS

Independent Variables

The topographic variables elevation, slope, aspect and northness were obtained from C-band radar altimetry flown aboard the space shuttle Endeavor as part of the National Aeronautics and Space Administration's Shuttle Radar Topography Mission (SRTM). The 27 m resolution SRTM Digital Elevation Model (DEM) was ingested into a Geographic Information System (GIS) and used to derive the slope and aspect. The northness parameter was derived from the product of the cosine of the aspect and the sin of the slope.

Average incoming solar radiation was calculated using TOPORAD (Dozier, 1980; Dozier and Frew, 1990). Using LOWTRAN7 (Kneizys *et al.*, 1998), the atmospheric transmission parameters that caused TOPORAD to match the observed incoming solar radiation values at the Emerald Lake and Topaz Lake meteorological stations were calculated (Dubayah, 1991). This was done for 5 different atmospheric conditions ranging from clear sky to cloud cover. Using these atmospheric parameters, TOPORAD was then used to distribute the incoming solar radiation across the basin. Each hourly solar radiation grid was averaged to derive the incoming solar radiation grid used as an independent variable in this study.

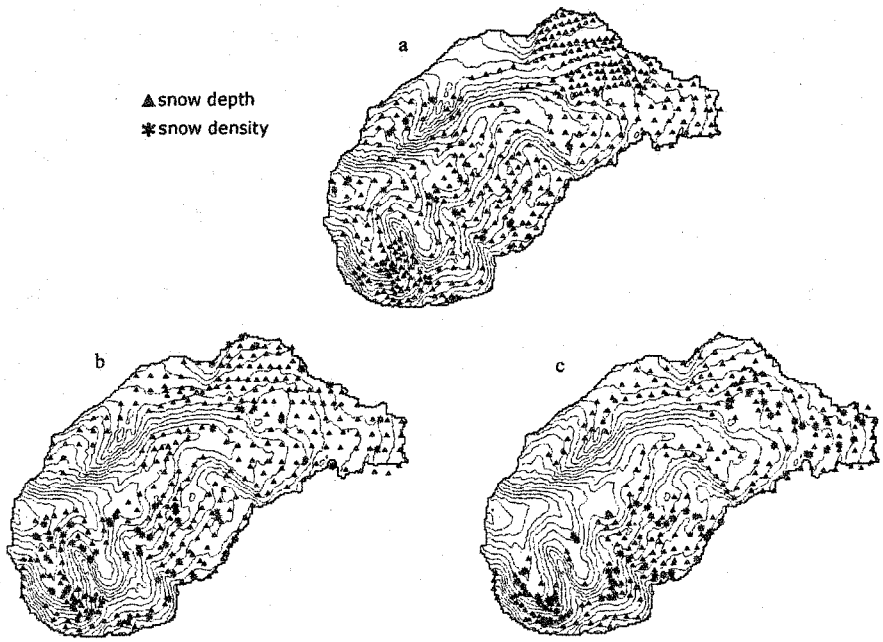

Figure 2. Snow depth and density sample locations for April (a), May (b), and June (c), 1997 in the Tokopah basin.

The maximum upwind slope (MAXUS) is a terrain-based parameter designed to capture the variability in snow deposition as a result of wind redistribution (Winstral *et al.*, 2002). A histogram of wind direction data from the Emerald Lake meteorological station was used to define the prevailing wind direction (Figure 3). A 90° pie shaped area centered on the prevailing wind direction with a radius of 100 m was used to define the upwind area of each source pixel (Figure 4). Within the upwind area, the algorithm searches along directional vectors at 5° increments to calculate the greatest upwind slope, S relative to the source cell, m:

$$S_{m,a,}(x_i y_i) \quad = max\left[tan\left(\frac{ELEV(x_v, y_v) - ELEV(x_i, y_i)}{\left[(x_v - x_i)^2 + (y_v - y_i)^2\right]^{0.5}} \right)\right]$$

where a is the azimuth of the directional search vector, $ELEV$ is elevation, (x_i,y_i) are the coordinates of the source cell, and (x_v,y_v) are the coordinates of all cells along the directional search vector. The MAXUS value of the source cell is the average maximum value of each vector within the upwind area:

$$MAXUS_m(x_i, y_i)\Big|_{a=220}^{a=310} = \frac{1}{n_v} \sum_{a=220}^{a=310} S_{m,a}(x_i, y_i)$$

where n_v is the number of search vectors within the search area.

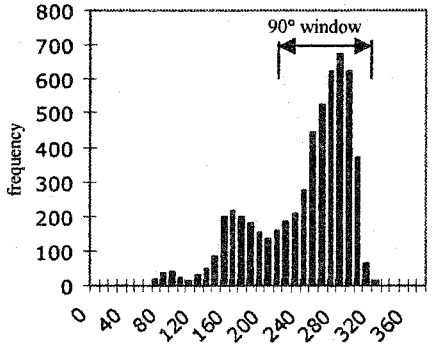

Figure 3. Histogram of wind direction measured at the Emerald Lake meteorological station from November 1, 1996 to June 20, 1997 with the 90° window used to define the upwind area from each source cell in the calculation of MAXUS.

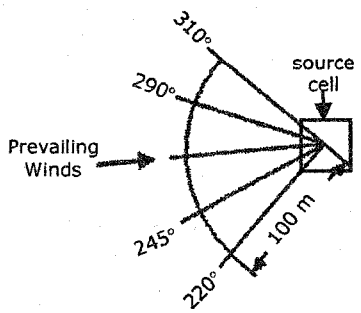

Figure 4. Pie shaped neighborhood used to calculate MAXUS. The algorithm searched along directional vectors at 5° increments (example vectors are shown for 310°, 290°, 265°, 245° and 220°) to calculate the greatest upwind slope relative to the source cell. MAXUS was determined as the average maximum value of all vectors within a 90° window surrounding the prevailing wind direction.

Binary Regression Trees

Binary regression tree models predict dependent variables from a suite of independent variables in a non-linear hierarchical fashion. Binary recursive partitioning is used to bin a dataset into increasingly homogeneous subsets. In this application various combinations of independent variables were included into separate tree models (Table 1). All of the models included elevation, solar radiation and maximum upwind slope as these variables have been shown to play an important role in snow distribution (Elder *et al.*, 1995, 1998, Balk and Elder, 2000, Erxleben *et al.*, 2002, Winstral *et al.*, 2002). For each combination of independent variables a tree was intentionally grown to over-fit the data as described in Chambers and Hastie (1993). Ten-fold cross-validation procedures were then used to generate plots of model deviance versus number of terminal nodes. Tree sizes that minimized model deviance were examined for further consideration. Trees were then grown with the number of terminal nodes restricted to all integer values between 2 and 30 and resultant coefficient of determination (R^2) plotted versus number of terminal nodes. The tree model that resulted in the lowest deviance and highest R^2 was then checked for unrealistic node splits and used to predict snow depth across the basin. These surfaces were then qualitatively compared to previous studies of snow distribution in the basin (Elder, 1995, Cline *et al.*, 1998). A detailed description of the tree fitting, pruning and cross-validation procedures can be found in Breiman *et al.* (1984), and an application to snow depth in Elder *et al.* (1995, 1998) and Balk and Elder (2000).

Table 1. Independent variables used in the 5 different regression tree models.

	model number				
independent variable	1	2	3	4	5
sol rad	Y	Y	Y	Y	Y
elevation	Y	Y	Y	Y	Y
maxus	Y	Y	Y	Y	Y
slope		Y	Y	Y	Y
aspect			Y	Y	
northness				Y	Y

Residual Interpolation

Inverse distance weighting, kriging and co-kriging, with the aforementioned independent variables, were used to distribute snow depth residuals from the regression tree models.

Inverse distance weighted interpolation predicts cell values using a linearly weighted combination of neighboring points, where the weight is based on the inverse of the distance between the predicted cell and the neighboring points. Typical use of IDW employs a weighting exponent of 2 but advances in GIS software have afforded easy calculation of an optimized weighting exponent, designed to minimize the RMSE of the interpolation. In this study two IDW approaches were applied and results compared. 1. Using an optimized weighting exponent, IDW_{opt}, and 2. using the squared exponent, IDW_2. For a detailed description of IDW see Isaaks and Srivastava (1989).

Geostatistical techniques have been used to distribute point snow depth values across regional scales (Carroll and Cressie, 1996) and at the basin scale (Hosang and Dettwiler, 1991). Kriging and co-kriging techniques have been used to distribute regression tree model snow depth residuals (Erxleben *et al.*, 2000, and Balk and Elder, 2000). As a preliminary step to kriging the spatial autocorrelation of the snow depth residuals was assessed using the Moran's I statistic (Kaluzny *et al.*, 1998). Kriging is based on fitting a model to the variogram to obtain weights that are used to assign values to unsampled locations. The variogram was calculated as:

$$\gamma(h) = \frac{1}{2m(h)} \sum_{i=1}^{m(h)} \left[Z(x_i) - Z(x_i + h) \right]^2$$

where $m(h)$ is the number of sample pairs separated by distance h, $Z(x_i)$ and $Z(x_i + h)$ are the residual value pairs at location x_i and $x_i + h$ respectively. Spherical, gaussian and exponential models were fit to the variogram and the model resulting in the lowest RMSE was selected.
The kriging interpolator was then applied:

$$\hat{Z}(x_0) = \sum_{i=1}^{n} \lambda_i Z(x_i)$$

where $\hat{Z}(x_0)$ is the estimate of the residual snow depth at location x_0, λ_i is the weight assigned to the known snow depth residual $Z(x_i)$ at location x_i. The sum of the weights, λ_i, must equal 1.

The dependent variable snow depth is known to vary as a function of independent variables such as elevation, slope and incoming solar radiation. Thus, some cross-correlation between these variables may exist and the use of co-kriging becomes attractive. As a preliminary step to co-kriging, cross-variograms were developed between the snow depth residuals and each independent variable (i.e. co-variable):

$$\gamma_{zw}(h) = \frac{1}{2m(h)} \sum_{i,j=1}^{m(h)} [Z(x_i) - Z(x_i + h)] [w(x_j) + w(x_j + h)]$$

where w is the value of the co-variable at location x_j.

Once the cross-variograms were calculated co-kriging models were developed using spherical, gaussian and exponential model fits. As with kriging, the model fit resulting in the lowest RMSE was selected.

The co-kriging interpolator was then applied:

$$\hat{Z}(x_0) = \sum_{i=1}^{n} \lambda_i^Z Z(x_i) + \sum_{j=1}^{m} \sum_{i=1}^{n} \lambda_j^w w(x_j)$$

where $\hat{Z}(x_0)$ is the estimate of the residual snow depth at location x_0, λ_i^Z is the weight assigned to the known snow depth residual, $Z(x_i)$, at location x_i, and λ_j^w is the weight assigned to the known co-variable value, $w(x_j)$ at location x_j. The sum of the weights, λ_i^Z and λ_j^w must equal 1 and 0 respectively. Detailed descriptions of the procedures described above can be found in Isaaks and Srivastava (1989).

The accuracy of the residual interpolation methods was assessed by jack-knifing each data point and deriving an error value for each observation. Results of each residual interpolation method were compared to the optimal regression tree model to assess whether or not the residual interpolation improved the results of the regression tree. Statistical comparisons were done using the mean absolute error, the RMSE and the coefficient of determination (R^2) of each model.

Snow Density

Snow density varies much less than does snow depth, making complex modeling unwarranted (Elder, 1995). Additionally, complex techniques are unwarranted because of the small density sample size and poor correlation with independent variables. Multi-variate linear regression models were developed between observed snow density and all aforementioned independent variables. A correlation coefficient matrix was calculated to identify variables that were significantly correlated with snow density. Using the correlated independent variables, regression models were developed. R^2 values and analyses of variance were used to assess model performance. IDW was also used to explain the variability in snow density. The R^2 statistic was used to determine if the IDW models could be used.

Snow Covered Area

Satellite imagery from the Landsat Thematic Mapper (TM) on April 6, June 9, and June 25 1997 were used to construct fractional snow covered area (SCA) images across the basin using the spectral mixture analysis algorithm of Rosenthal and Dozier (1996). Imagery from the Airborne Visible and Infrared Imaging Spectrometer (AVIRIS) was also used to obtain fractional SCA data on May 8, 1997 using the spectral mixture analysis model for subpixel SCA, grain size, and albedo described by Painter *et al.* (2003). The April 6 and May 8 SCA images were acquired on the first day of each respective snow survey. The June 9 and June 25 SCA images were averaged to obtain fractional SCA estimates corresponding to the time of the June snow survey (i.e. June 18). The 30 m resolution SCA surfaces were scaled to 0 – 1 for use in the SWE calculations described below.

Snow Water Equivalent

For each simulation the *SWE* of each pixel, p, within the basin was determined:

$$SWE_p = d_p \times (\rho_s \div \rho_w) \times SCA_p$$

Where d_p (m) is the modeled snow depth, ρ_s (kg m^{-3}) is the modeled snow density and ρ_w is the density of water (1000 kg m^{-3}).

RESULTS

Field Observations

The mean snow depth of each snow survey decreased from April to June while snow density increased over the same period (Table 2). Snow depth variability increased throughout the melt season while snow density variability decreased from April to May and increased slightly from May to June (Table 2). Snow depth variability was considerably greater than that for snow density (Table 2).

Table 2. Summary statistics for snow depth (cm) and snow density (kg m^{-3}) field measurements including standard deviation, std. dev., coefficient of variation, cv, and sample size, n.

	April		May		June	
	density	depth	density	depth	density	depth
minimum	252	0	384	0	421	22
maximum	517	795	652	540	743	454
mean	422	255	520	168	600	128
std. dev.	70	97	46	85	63	67
cv	0.17	0.38	0.09	0.51	0.11	0.52
n	19	397	76	303	66	258

Binary Regression Trees

Results from the cross validation showed that model deviance was minimized when solar radiation, elevation, MAXUS and northness were used as independent variables for all simulations (Figure 5a). Model fit improved with the addition of northness for all of the simulations as shown by the plots of coefficient of determination (R^2) versus number of terminal nodes (Figure 5b). Improvements in R^2 for the June simulation were not found for smaller tree sizes (i.e. below 10 terminal nodes) (Figure 5b) and therefore northness was not used to construct the final tree for June. All of the other models listed in Table 1 yielded model deviances and model fits somewhere between the extremes shown in Figure 5 (plots not shown).

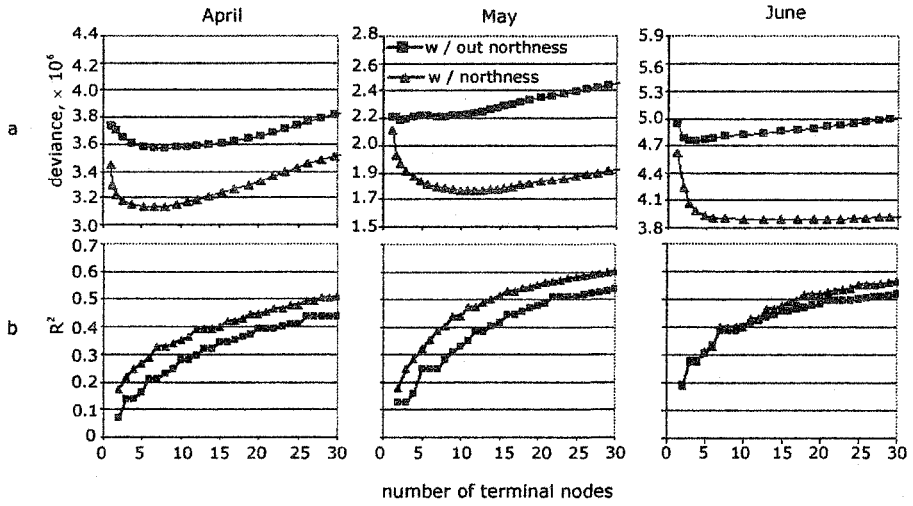

Figure 5. Model deviance (a) and coefficient of determination (R^2) (b) versus number of terminal nodes for regression tree models with and without northness. All models included elevation, average incoming solar radiation, and maximum upwind slope.

Results of the cross-validation indicated optimal tree sizes of 8, 11 and 10 nodes for the April, May and June simulations respectively (Figures 6a-c). The importance of the different independent variables is indicated by the order at which they appear in the tree (Elder, 1995). The April tree was able to explain 33% of the variability of snow depth with an RMSE of 79.4 cm (Table 3). The May tree was able to explain 48% of the variability while the June tree explained 40% of the snow depth variability. RMSE values for the May and June simulations were 62.2 cm and 52.6 cm respectively (Table 3).

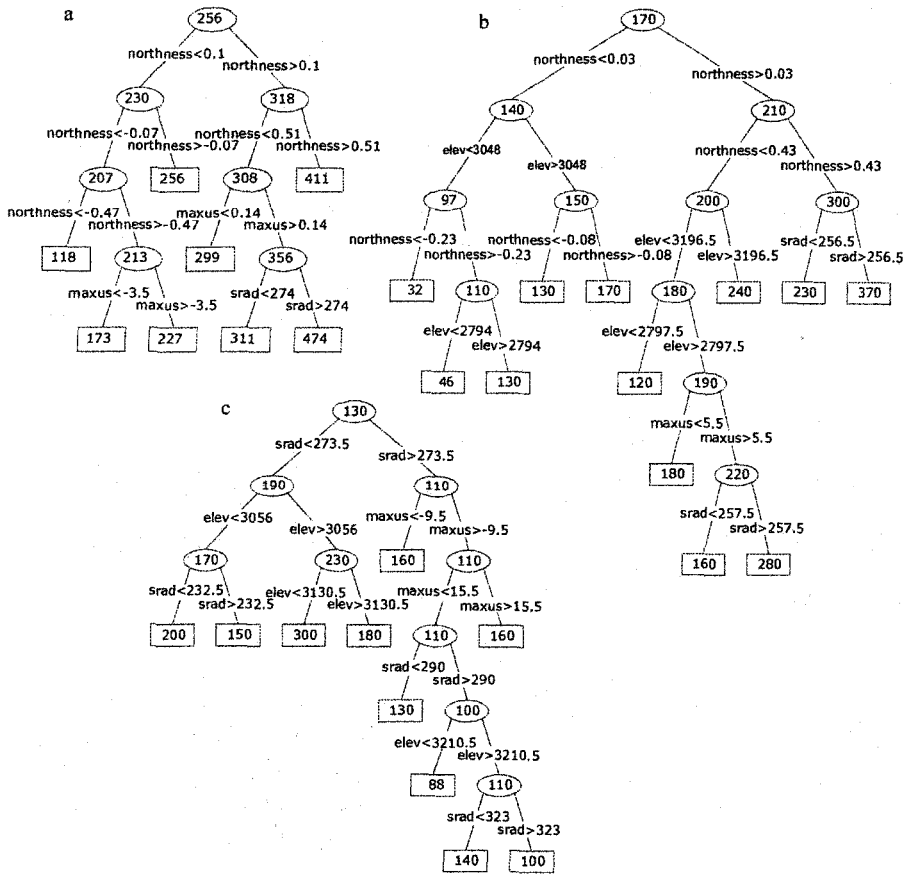

Figure 6. Regression tree snow depth (cm) models for April (a), May (b) and June (c), 1997 in the Tokopah basin.

Table 3. Mean absolute error (MAE), root mean square error (RMSE), and coefficient of determination (R^2) values for all snow depth interpolation models, Tokopah basin, 1997.

	April			May			June		
Model	MAE	RMSE	R^2	MAE	RMSE	R^2	MAE	RMSE	R^2
regression tree	61.65	79.41	0.33	47.47	62.19	0.48	40.02	52.57	0.40
IDW	62.15	80.37	0.33	46.40	60.89	0.50	41.18	55.01	0.36
IDW-OPT	59.86	76.97	0.38	45.37*	59.54*	0.52*	40.23	53.36	0.39
krig	61.78	80.09	0.34	45.55	59.97	0.51	39.45	52.07	0.41
co-krig, srad	58.12*	76.18*	0.39*	45.60	60.04	0.51	39.45*	52.06*	0.41*
co-krig, slope	58.56	76.57	0.38	45.59	60.04	0.51	39.45	52.06	0.41
co-krig, northness	58.76	76.40	0.39	45.60	60.04	0.51	39.44	52.06	0.41
co-krig, maxus	58.14	76.18	0.39	45.59	60.04	0.51	39.45	52.07	0.41
co-krig, elevation	58.14	76.18	0.39	45.60	60.04	0.51	39.45	52.06	0.41

*best model

Residual Interpolation

Snow depth residual interpolation for April improved model fit by 1.7% to 18%, with IDW_2 yielding the poorest results and co-kriging with solar radiation giving the best results (Table 3). For the April simulation optimization of the IDW exponent to a value of 1.09 resulted in an improvement over IDW_2 but not over the co-

kriging models. April RMSE values increased when kriging and IDW_2 were used to model the distribution of the model residuals (Table 3). Co-kriging with solar radiation decreased the April RMSE by 4%. The April Moran's I value ($p = 0.024$) indicated that the residuals were spatially auto-correlated ($p < 0.05$). Hence kriging models performed more accurately than the IDW models. April variograms and cross-variograms for snow depth residuals and solar radiation are shown in Figure 7a-c.

May model fit increased by 5.3% to 8.8% using the different residual interpolation methods, with IDW_2 yielding the poorest results and IDW_{opt}, with an exponent of 1.27, the best results (Table 3). May RMSE values decreased by 4.3% and 2.1% for the IDW_{opt} and IDW_2 models respectively. May RMSE values decreased by 3.5% on average using the different co-kriging and kriging models. The Moran's I value ($p = 0.103$) was not significant at the 0.05 level, indicating that the May residuals were not spatially auto-correlated. Hence IDW_{opt} performed better than the kriging and co-kriging models. May variograms and cross-variograms for snow depth residuals and solar radiation are shown in Figure 7d-f.

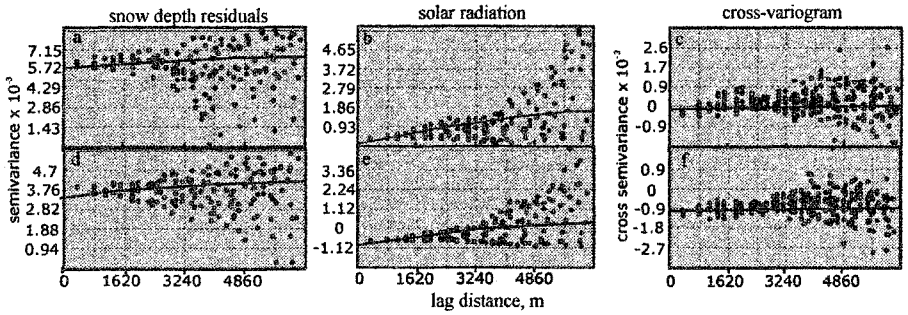

Figure 7. Variograms fit with spherical models and cross-variograms fit with gaussian models for snow depth residuals and solar radiation for the April (a –c) and May, 1997 (d-f) interpolations.

June R^2 values increased by 3.1% using all of the kriging and co-kriging models. Co-kriging with solar radiation performed slightly better then the other geostatistical methods for the June simulation (Table 3). June R^2 values decreased using both of the IDW models (Table 3). June RMSE values decreased by only 1% using co-kriging with solar radiation, while RMSE values increased for both of the IDW models (Table 3). The June Moran's I ($p = 0.08$) was not significant at the 5% confidence level however it was significant at the 10% confidence level indicating that slight spatial auto-correlation of residuals exists.

Snow Density

The independent variables northness and slope only explained 22% of the April variability. The Analysis of variance (ANOVA) F-statistic (Ott, 1993) was not significant at the 5% confidence level ($p = 0.154$). MAXUS and slope explained only 11% of the snow density variability for May. ANOVA results were significant at the 5% level ($p = 0.05$). Solar radiation and slope explained 10% of the variability for June; with ANOVA results significant at the 5% level ($p = 0.043$). Poor model results may be a result of sampling errors caused by inconsistent use of the Federal Sampler. The standard error of the estimates were 6%, 4%, and 3% lower than the standard deviations of the April, May and June observations respectively. Lower R^2 values were obtained using IDW with an exponent of 2. Given the poor results of the attempted models, the mean observed snow density value of each snow survey was used in the SWE calculation as per Erxleben *et al.* (2002).

Snow Covered Area

SCA decreased throughout the snowmelt season (Figure 8). SCA decreased by 6% between the April and May snow surveys and by 62% between the May and June surveys.

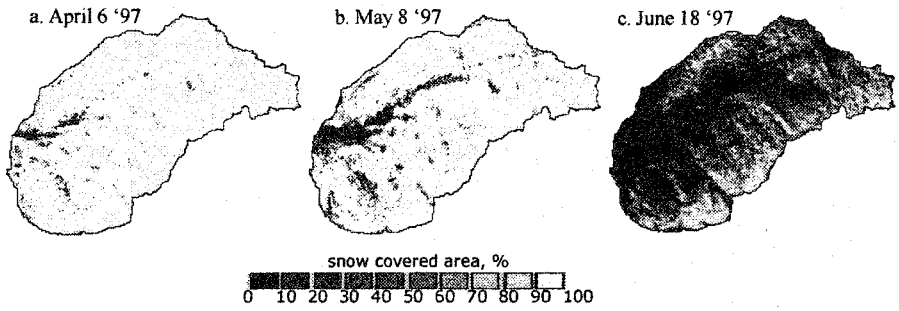

Figure 8. Fractional snow covered area for the Tokopah basin from the Landsat Thematic Mapper (a,c) and the Airborne Visible/Infrared Imaging Spectrometer (b).

Snow Water Equivalent

The mean April SWE was the same for all of the geostatistical techniques, with IDW_{opt} resulting in a negligible decrease in SWE (Table 4). Maximum April SWE was considerably higher using IDW_{opt} and thus the standard deviation and the coefficient of variation was slightly above the values obtained using geostatistical techniques. April SWE distributions showed a distinct difference between the higher SWE accumulations in areas south of the valley floor relative to areas north of the valley floor (Figure 9a). Especially high SWE was predicted on the northeast facing slopes of areas south of the valley floor because of lower incoming solar radiation and leeward slope orientation.

Table 4. Statistical summaries for April, May, and June, 1997 SWE simulations for the Tokopah basin. Statistics shown are the resultant values when the three best geostatistical techniques and the best IDW techniques were used to distribute residual snow depths. The minimum value of all of the simulations was 0.

	April				May				June*		
	cokrig-elev	cokrig-maxus	cokrig-srad	IDW_{opt}	cokrig-maxus	cokrig-slope	kriging	IDW_{opt}	cokrig-north	cokrig-srad	cokrig-elev
maximum	230.14	230.01	229.77	266.78	220.92	221.14	220.92	280.41	166.51	166.15	166.15
mean	105.48	105.49	105.49	105.20	79.42	79.43	79.42	79.79	26.29	26.27	26.27
std. dev.	30.27	30.27	30.31	31.55	38.54	38.56	38.54	39.13	26.86	26.83	26.83
cv	0.29	0.29	0.29	0.30	0.49	0.49	0.49	0.49	1.02	1.02	1.02

*IDW not used because of poor results.

Mean SWE using IDW_{opt} was greater than the mean SWE of all of the geostatistical techniques during May (Table 4). The maximum value and standard deviation was also greater for IDW_{opt}. The spatial distribution of May SWE showed a similar pattern to that of April (Figure 9b). The mean SWE decreased from the April simulation but the standard deviation increased. SWE differences across the basin are visually more pronounced than April.

All of the geostatistical techniques produced similar SWE statistics for June (Table 4). IDW interpolation of snow depth residuals was not used to generate modeled SWE distributions in June because of the poor result of the method. June SWE distribution became somewhat uniform in areas where snow remained (Figure 9c) and the standard deviation decreased from the May value (Table 4).

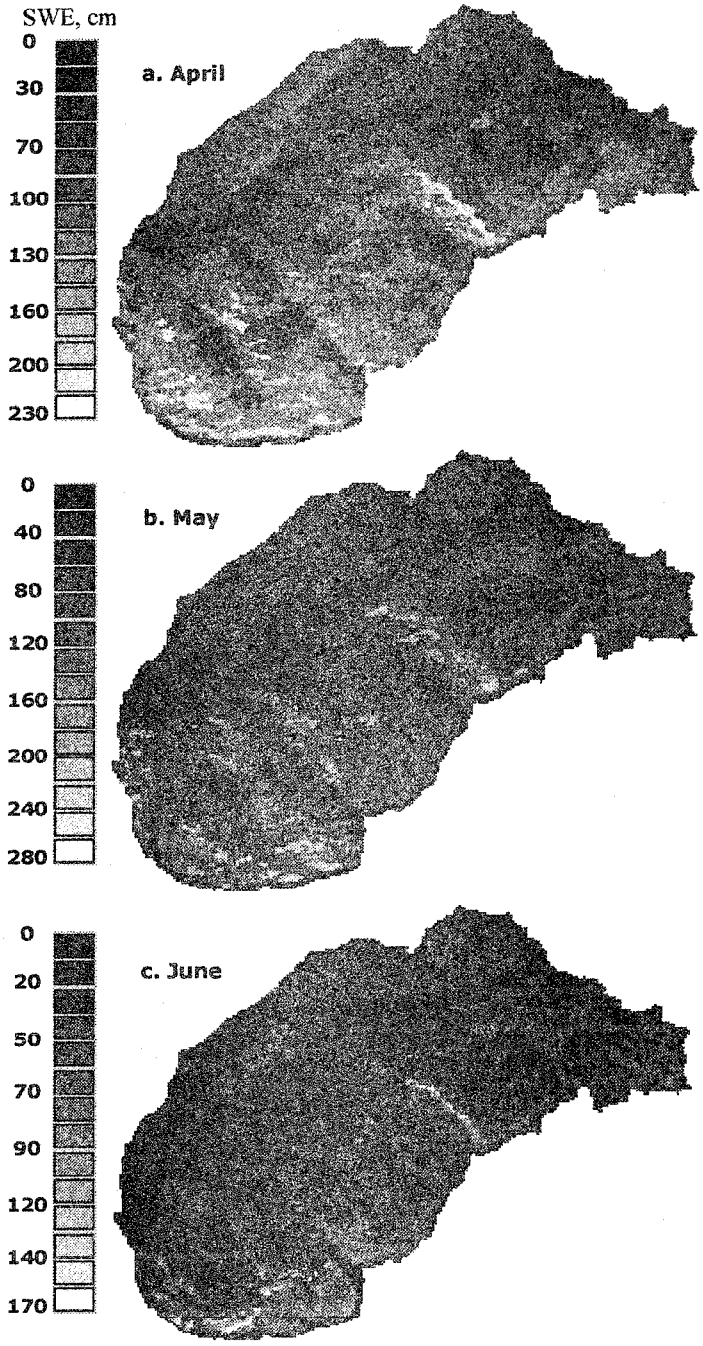

Figure 9. Distributed SWE estimates for the Tokopah basin, 1997.

DISCUSSION

Binary Regression Trees

Binary regression trees have been used to estimate the spatial distribution of snow depth in complex topography like that of the Tokopah basin with considerable success in some cases (Balk and Elder, 2000, Elder *et al.*, 1995) and marginal success in others (Erxleben *et al.*, 2002). It is particularly challenging to capture factors that result in leeward slopes accumulating several meters of snow, while nearby windward slopes become snow-free due to wind scour. Previous studies are not directly comparable given that the coefficient of determination (R^2) is the measure of model success commonly used and R^2 increases with increasing number of terminal nodes (Figure 5b) (Erxleben, 2002, Winstral *et al.*, 2002, Balk and Elder, 2000, Elder, *1995,* Elder *et al.*, 1995). Thus, comparing only R^2 values becomes subjective because different tree sizes are used for different applications. Nevertheless quantitative comparisons are useful when associated caveats are stated. The average regression tree model fit (R^2 of 0.44) of this research was encouraging relative to other studies. Model fit was considerably better than the results of Erxeleben *et al.* (2002) (average R^2 = 0.25). Differences are likely due to the fact that, in the alpine terrain of this study, the independent variables were better able to explain snow distribution patterns than in the forested terrain of Erxleben's study in the Colorado Rocky Mountains. Balk and Elder (2000) yielded better results (R^2 = 0.59) than obtained in this study but in a much smaller catchment (6.9 km^2) and using an 18 terminal node regression tree.

The issue of catchment size is not trivial. Snow distribution patterns of two small adjacent catchments may not correlate with independent variables in the same manner because the processes controlling snow distribution are only applicable over a narrow range of conditions (Elder, 1995). Elder (1995) found that 10-node regression trees applied in the Tokopah basin in 1993 and 1994 yielded average R^2 values of 0.40, while tree models constructed for sub-basins of the Tokopah, ranging from 0.69 to 1.78 km^2 in area, yielded R^2 values ranging from 0.6 to 0.8. The average R^2 value of 0.44 obtained in this research is therefore considered an improvement over the work of Elder (1995) and could be considered comparable to R^2 values in the range of 0.6 to 0.8 for catchments with areal extents less than or equal to approximately 2 km^2.

Winstral *et al.* (2002) improved model fit from an R^2 of 0.35 to 0.5 with the addition of terrain parameters designed to capture the variability in snow depth due to wind redistribution. The results presented here compare well considering that Winstral's work was done in a 2.25 km^2 basin. In addition to the difference in scale, the lower R^2 values obtained in this research may be due to the fact that in the Tokopah basin wind redistribution of snow occurs only during and immediately following snowfall due to the warm air temperatures of the region (Elder, 1995), whereas in Winstal's continental study area wind redistribution of snow may persist for a much longer period of time after snowfall.

This research has built upon the aforementioned applications by showing that in addition to MAXUS, additional terrain variables (i.e. northness) requiring minimal computational effort can further improve model results. The need for the northness variable arose when regression tree results without the northness variable resulted in snow depth overestimates in the northwestern region of the basin known as the north valley (Figure 10a). The extent of the overestimates became apparent when the snow depth estimates were qualitatively compared to previous studies of snow distribution in the Tokopah basin (Elder, 1995). Addition of the northness variable removed this problem and resulted in lower overall model deviance (Figure 5a), improved model fit (Figure 5b) and removal of the overestimates in the north valley (Figure 10b).

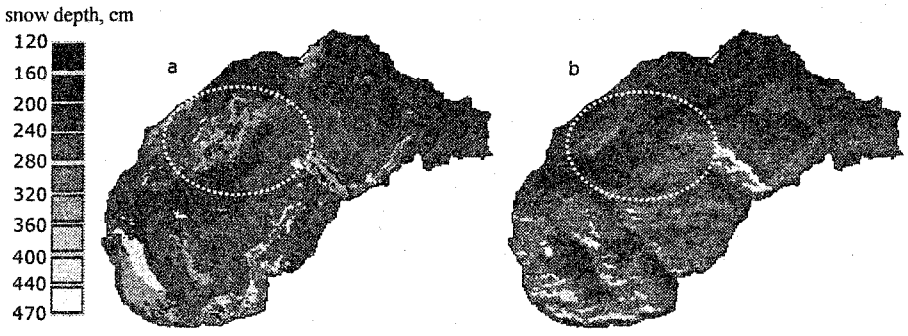

Figure 10. Distributed snow depth estimates from binary regression trees for April, 1997 using average incoming solar radiation, elevation, and maxus (a), and with the addition of northness (b). The ellipse indicates the North Valley where snow depth was overestimated without northness.

The lower model fit obtained in April ($R^2 = 0.33$) may be due to the fact that the processes controlling snow distribution can be statistically modeled more accurately when snowmelt begins to play a significant role in snow distribution. This is supported by the absence of elevation in the April tree (Figure 6a); elevation does not seem to play a large role in snow distribution in the Tokopah basin until later in the snowmelt season when snowmelt begins in the lower elevations. Elevation appears on the second tier in the May and June regression trees (Figure 6b,c).

Residual Interpolation

This research has shown that simplistic residual interpolation techniques, such as IDW_{opt}, can give better results than complex techniques, such as Kriging and Co-kriging, when residuals are not spatially auto-correlated. Previous applications have not used IDW to distribute regression tree residuals to simulate snow depth. Geostatistical techniques performed better than IDW_{opt} for April and June but the average difference in the RMSE of these simulations was only 2%, suggesting that sufficient results are obtained using the more simplistic IDW approach (Table 4). Furthermore, the use of IDW_{opt} made an average difference of only 0.4% in the basin-wide mean SWE.

The substantial difference in the range of the SWE surfaces (12% higher on average using IDW_{opt}) is due to inherent differences in the interpolation procedures; IDW will not over or under estimate the input data, but it can approach the max and min values, creating a surface that has hills and valleys about the data points. Depending on the power used in IDW, nonlinear upward or downward trends in the surface will extend to the data points from the regional average. The co-kriging process creates a smoother surface than IDW_{opt}, in which the upward and downward trends are "cut off" (*D. P. Guertin, University of Arizona, personal communication, 2003*). The smoothing is inherent when fitting the model to the semivariogram, with the co-variable adding to the smoothing.

CONCLUSIONS

This research has shown that, in addition to previously used independent variables, northness can improve binary regression trees by increasing the model fit and minimizing overall model deviance. The utility of northness should not be unique to the Tokopah basin and further investigation is warranted in other regions. Using IDW_{opt} to distribute model residuals is a viable alternative to co-kriging techniques and may improve model accuracy when residuals are not spatially auto-correlated. The models predicted significantly more SWE in southern portions of the basin, with spatial variability decreasing throughout the snowmelt season. SWE distributions were predicted at accuracy levels quantitatively and qualitatively comparable to previous studies.

ACKNOWLEDGEMENTS

Financial support was provided by NASA's EOS Interdisciplinary Investigation on *Hydrology, Hydrochemical Modeling, and Remote Sensing in Seasonally Snow-Covered Alpine Drainage Basins* (NAG-4514) and by the National Science Foundation's Center for the Sustainability of semi-Arid Hydrology and Riparian Areas (SAHRA) (NSF EAR9876800). Ray Brice, Kelly Elder, Jennifer Erxleben, Walter Rosenthal and Damon Turney provided technical advice. Adam Winstral provided assistance with deriving MAXUS. Tom Painter provided the AVIRIS data. The field data collection teams are acknowledged with great respect.

REFERENCES

Balk B, Elder K. 2000. Combining binary decision tree and geostatistical methods to estimate snow distribution in a mountain watershed. *Water Resour. Res.*, **36**(1): 13-26.

Breiman L, Friedman J, Olshen R, Stone C. 1984. *Classification and Regression Trees*. Wadsworth and Brooks: Pacific Grove, Ca; 358.

Chambers JM, Hastie TJ. 1993. *Statistical models in S*. Chapman and Hall: London, UK, 608.

Carroll SS, Cressie N. 1996. A comparison of geostatistical methodologies used to estimate snow water equivalent, *Water Resour. Bulletin* **32**(2): 267-278.

Cline DW, Bales RC, Dozier J. 1998. Estimating the spatial distribution of snow in mountain basins using remote sensing and energy balance modeling, *Water Resour. Res.*, **34**(5): 1275-1285.

Dozier J. 1980. A clear-sky spectral solar radiation model for snow-covered mountainous terrain. *Water Resour. Res.*, **16**, 709-718.

Dozier J, and Frew J. 1990. Rapid calculation of terrain parameters for radiation modeling from digital elevation data, *IEEE Trans. Geos. Rem. Sens.*, **28**(5): 963-969.

Dubayah R. 1991. Using LOWTRAN7 and field flux measurements in an atmospheric and topographic solar radiation model. *Proceedings IGARSS*, 39-42, IEEE 91CH2971-0.

Elder K. 1995. Snow distribution in alpine watersheds. Ph.D. dissertation, 309 pp., Univ. of Calif., Santa Barbara.

Elder K, Michaelsen J, Dozier J. 1995. Small basin modeling of snow water equivalence using binary regression tree methods. *Biogeochemistry of Seasonally Snow-Covered Catchments*, edited by K.A. Tonnessen et al., *IAHS Publ.*, **228**: 129-139.

Elder K, Rosenthal W, Davis RE. 1998. Estimating the spatial distribution of snow water equivalence in a montane watershed. *Hydrol Process.*, **12**: 1793-1808.

Erxleben J, Elder K, Davis RE. 2002. Comparison of spatial interpolation methods for estimating snow distribution in the Colorado Rocky Mountains. *Hydrol. Process.*, **16**: 3627 – 3649.

Hosang J, Dettwiler K. 1991. Evaluation of a water equivalent of snow cover map in a small catchment area using a geostatistical approach, *Hydrol. Process.* **5**: 283-290.

Isaaks EH, Srivastava RM. 1989. *Introduction to Applied Geostatistics.* Oxford University Press: New York, NY, 538.

Kaluzny SP, Vega SC, Cardoso TP, Shelly AA. 1998. *S+ Spatial Stats: user's manual for Windows and Unix.* Springer: New York, NY, 327.

Kneizys FX, Shettle EP, Abreu LW, Chetwynd JH, Anderson GP, Gallery WO, Selby JE, Clough SA. 1988. User's Guide to LOWTRAN7. Report AFGL-TR-88-0177, Air Force Geophysics Laboratory, Bedford, MA.

Ott RL. 1993. *An Introduction to Statistical Methods and Data Analysis.* Wadsworth Inc.: Belmont, Ca., 1038.

Painter TH, Dozier J, Roberts DA, Davis RE, Green RO. 2003. Retrieval of subpixel snow-covered area and grain size from imaging spectrometer data. *Rem. Sens. Environ.* **85**: 64-77.

Rosenthal W, Dozier J. 1996. Automated mapping of montane snow cover at subpixel resolution from the Landsat Thematic Mapper. *Water Resour. Res.* **32**: 115-130.

Tonnessen KA. 1991. The Emerald Lake watershed study: introduction and site description, *Water Resour. Res.*, **27**(7): 1537-1539.

Winstral A, Elder K, Davis RE. 2002. Spatial snow modeling of wind-redistributed snow using terrain-based parameters. *J. Hydrometeorology*: **3** (5): 524-538.